The connection between star-formation rate and supermassive Black Hole accretion in the local Universe

Olena Torbaniuk[1*], Maurizio Paolillo[1,2,3], Giuseppe Longo[1,3], Cristian Vignali[4,5], Michele Delli Veneri[1,2], Stefano Cavuoti[1,2,3]

[1]Department of Physics, University of Napoli Federico II, via Cinthia 9, 80126, Napoli, Italy
[2]INAF — Osservatorio Astronomico di Capodimonte, via Moiariello 16, 80131, Napoli, Italy [3]INFN — Sezione di Napoli, via Cinthia 9, 80126, Napoli, Italy
[4]Department of Physics and Astronomy, University of Bologna, via Piero Gobetti 93/2, I-40129 Bologna, Italy
[5]INAF — Osservatorio di Astrofisica e Scienza dello Spazio di Bologna, via Piero Gobetti 93/3, I-40129 Bologna, Italy
*torbaniuk@fisica.unina.it

Introduction

An important problem in extragalactic astronomy concerns the influence of Active Galactic Nuclei (AGN) on the host galaxy and the correlation between the evolution of the host galaxy and the supermassive black hole (SMBH) in its centre. This connection between galaxies and SMBHs is suggested by the correlation between the masses [4, 5], and the similarity in the cosmological evolution of SFR and AGN activity.

The optical galaxy sample

We used the catalogue of galaxy properties from the 8th Data Release of Sloan Digital Sky Survey (SDSS DR8) performed by MPA–JHU group (*galSpec* catalogue) [3], which contains about 2 million galaxies within the redshift $z \leq 0.33$. Firstly, all objects with reliable values of the star-formation rates (SFR) and the total stellar masses ($\mathcal{M}_*$) were selected. All duplicates of the galaxies were rejected and we selected objects with reliable photometry in SDSS r- and i-bands. The resulting optical sample contains 538 317 galaxies.

The X-ray sample

To quantify the accretion onto SMBH we used data from XMM-Newton Serendipitous Source Catalogue (3XMM DR8) [8]. The crossmatch of 3XMM DR8 with our optical sample compiled from *galSpec* catalogue (with a matching radius of 5″) gives 1684 X-ray counterparts. We rejected all objects with the detection flag SUM_FLAG > 3 and a non-zero extension parameter to avoid including spatially extended objects (such as hot gas regions or galaxy clusters), respectively. The final X-ray sample contains 1477 objects.

The X-ray data

The XMM catalogue contains the observations from three cameras PN, MOS1 and MOS2. For our study we selected detections from the most sensitive PN camera. For objects with multiple observations we choose the one with the highest exposure time. When the data from PN camera were missing we used those from MOS1 or MOS2 cameras.

Rest-frame X-ray fluxes we computed in the full band (0.2 to 12 keV), soft band (0.5–2.0 keV) and hard band (2.0–12 keV) after applying a K-correction (we assumed a photon index $\Gamma = 1.4$ appropriate for medium obscuration AGN spectrum shape). Since X-ray radiation for the objects in our sample can be partially emitted by X-ray binaries and SNe in the host galaxy it is important to calculate the fraction of such X-ray emission and reject it to obtain the contribution of the AGN. The X-ray luminosity of SF regions was determined using the relation between $L_{X,SF}$ and SFR from [6] (in soft and hard bands) and (full band). The redshift distribution of our final sample after corrections is shown in Fig. 1. To compute the BHAR we used only the hard X-ray band since it is more sensitive to AGNs emission and allows to avoid the contamination from star-formation radiation.

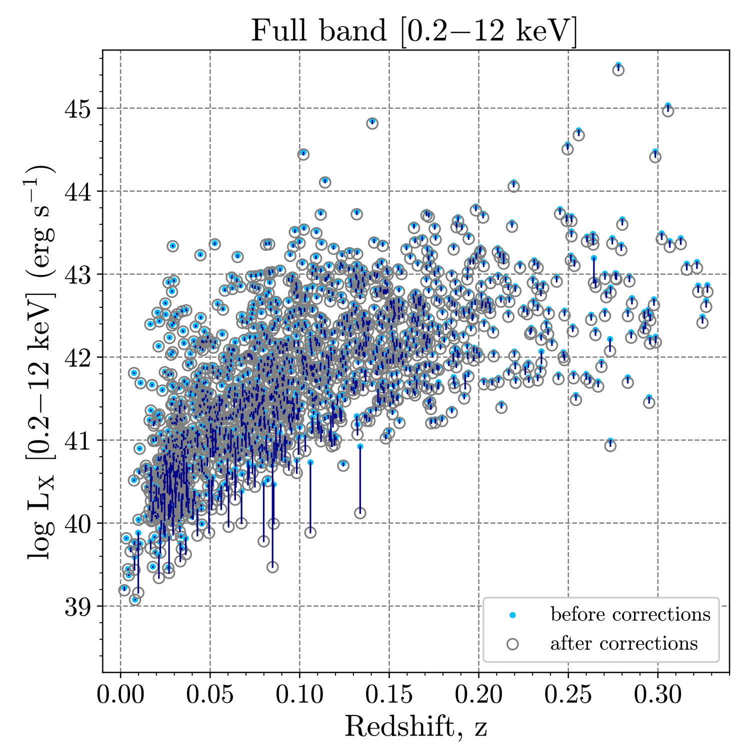

Figure 1: The redshift distribution of X-ray luminosity of 1477 objects from our 3XMM sample. Blue filled circles are the values of L_X before K-correction and substraction of X-ray emission from star-formation, grey open circles — the values of L_X after corrections. The shift in L_X for each object is shown by a solid line.

AGN selection

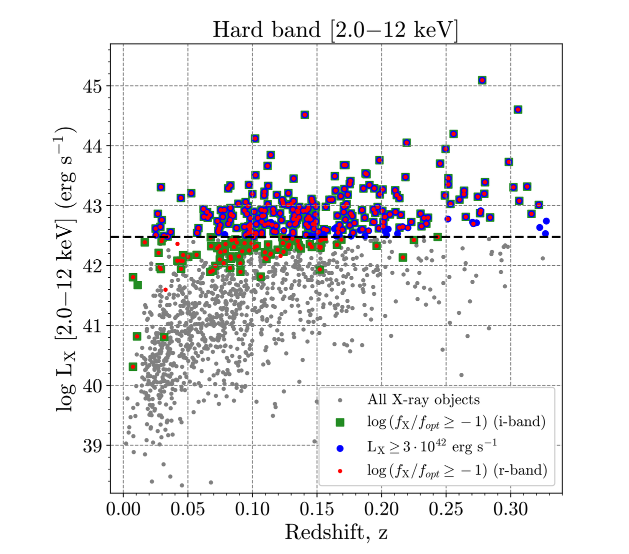

Figure 2: The X-ray luminosity vs. redshift for the objects in X-ray sample (grey dots). The horizontal dashed line indicates $L_X \geq 3 \cdot 10^{42}$ erg s^{-1} criteria utilized to classify AGNs. Red circles and green squares represent AGNs selected by X-ray/optical flux ratio criteria in SDSS r- and i-bands, respectively (Fig. 3).

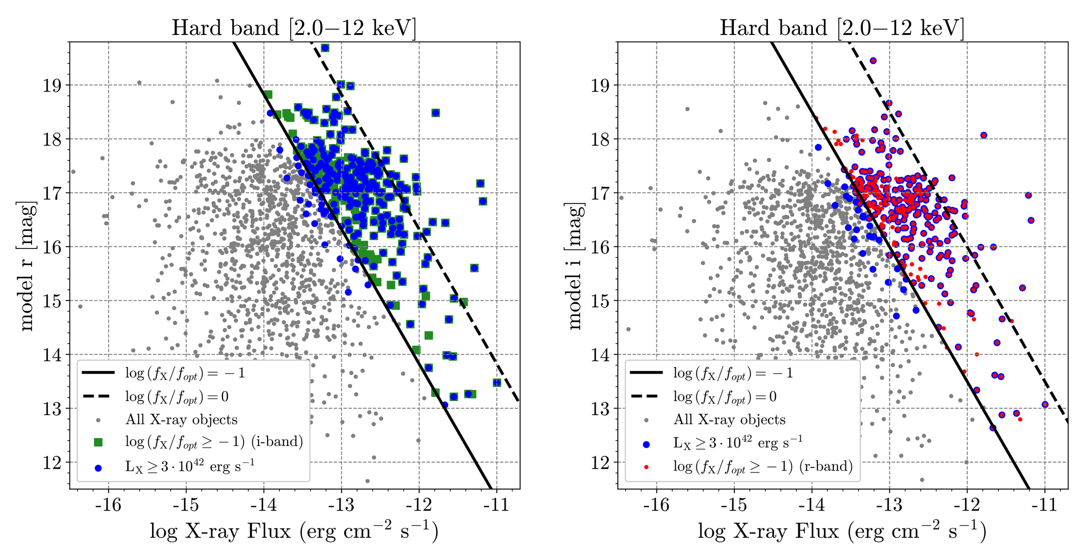

Figure 3: The X-ray flux in hard band vs. optical SDSS r-band (left panel) and i-band magnitude (right panel) for sources in our X-ray sample (grey circles). Blue circles indicate AGNs having $L_X \geq 3 \cdot 10^{42}$ erg s^{-1} (see Fig. 2). AGNs selected by the X-ray/optical flux ratios in SDSS r- and i-band are represented by red circles and green squares, respectively. Diagonal lines indicate constant flux ratios between the SDSS r- and i-band and X-ray hard band, the area under the line $\log(f_X/f_{opt}) \geq -1$ is used as one of the criteria to classify the location of AGNs.

SFRs of the galaxy with AGNs

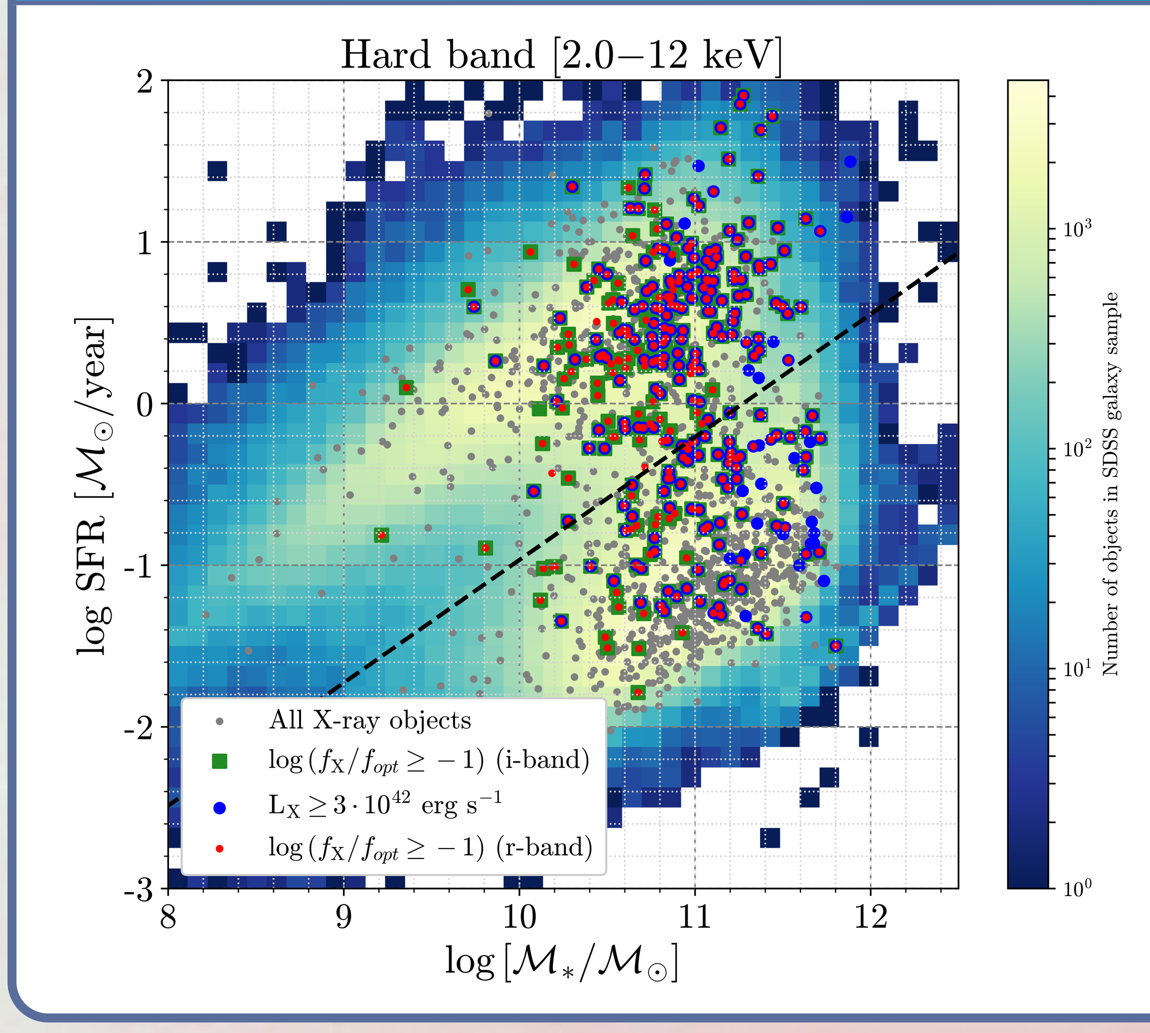

Figure 4: The distribution of star-formation rate vs. stellar mass for X-ray sample in hard band (grey circles). The gradient from blue to yellow shows the 2D histogram of the density distribution of galaxies in our optical SDSS sample. All symbols represent the AGNs selected by the criteria shown in Fig. 2, 3. Our galaxy sample was divided into star-forming (above black dashed line) and passive (below black dashed line) galaxies on the basis of their SFRs relative to the evolving main sequence from [1,2]. It is worth noticing that the AGNs selected with above criteria above are mainly located at range with $\log[\mathcal{M}_*/\mathcal{M}_\odot] > 10.0$. Also, the majority of AGNs occupy the star-forming main-sequence (above dashed line).

The specific black hole accretion rate (sBHAR)

As the sensitivity of X-ray observations covering our galaxy sample varies in depth (different exposure time, off-axis angle, detector) we have to correct our sample for the fraction of missed sources as a function of flux. For this purpose, we used the count/flux upper limit service for XMM data, XMM FLIX. We collected the values of the flux upper limit for each objects and compiled the cumulative curves which describe the likelihood of detecting the object with the corresponding X-ray flux using one of the XMM cameras (Fig. 5). This cumulative curves were applied as statistic weight to scale the number of objects in our distribution histograms (Fig. 6).

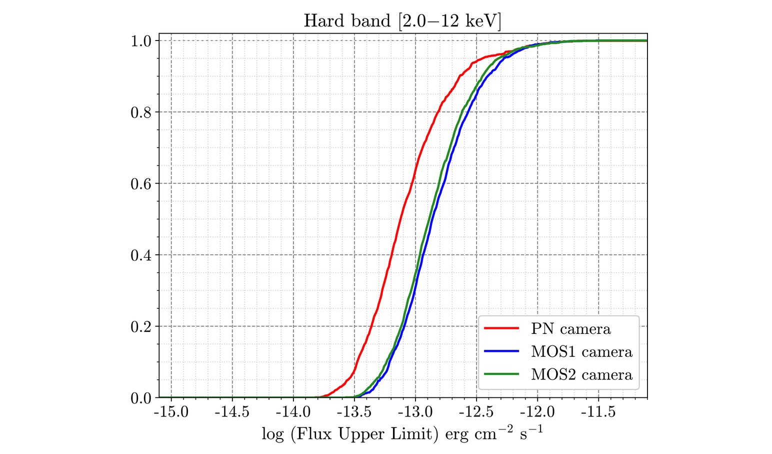

Figure 5: The cumulative histogram of flux upper-limit in hard band [2.0−12 keV] for XMM cameras from XMM FLIX service.

The specific black hole accretion rate ($\lambda_{\rm sBHAR}$) is the rate of accretion onto the central SMBH scaled relative to the stellar mass of the host galaxy and was calculated from [2] as

$$\lambda_{\rm sBHAR} = \frac{k_{bol} L_{\rm X,hard}}{1.3 \cdot 10^{38}\, {\rm erg\, s^{-1}} \times 0.002\, \mathcal{M}_*/\mathcal{M}_\odot},$$

where k_{bol} is a bolometric correction factor $k_{bol} = 25$ and $L_{\rm X,hard}$ is the 2.0–12 keV X-ray luminosity. The additional scale factors are chosen such that $\lambda_{\rm sBHAR} \approx \lambda_{\rm Edd}$, the Eddington ratio $\lambda_{\rm Edd} \propto L_X/\mathcal{M}_{\rm BH}$, assuming that mass of the central black hole scales directly with total host stellar mass.

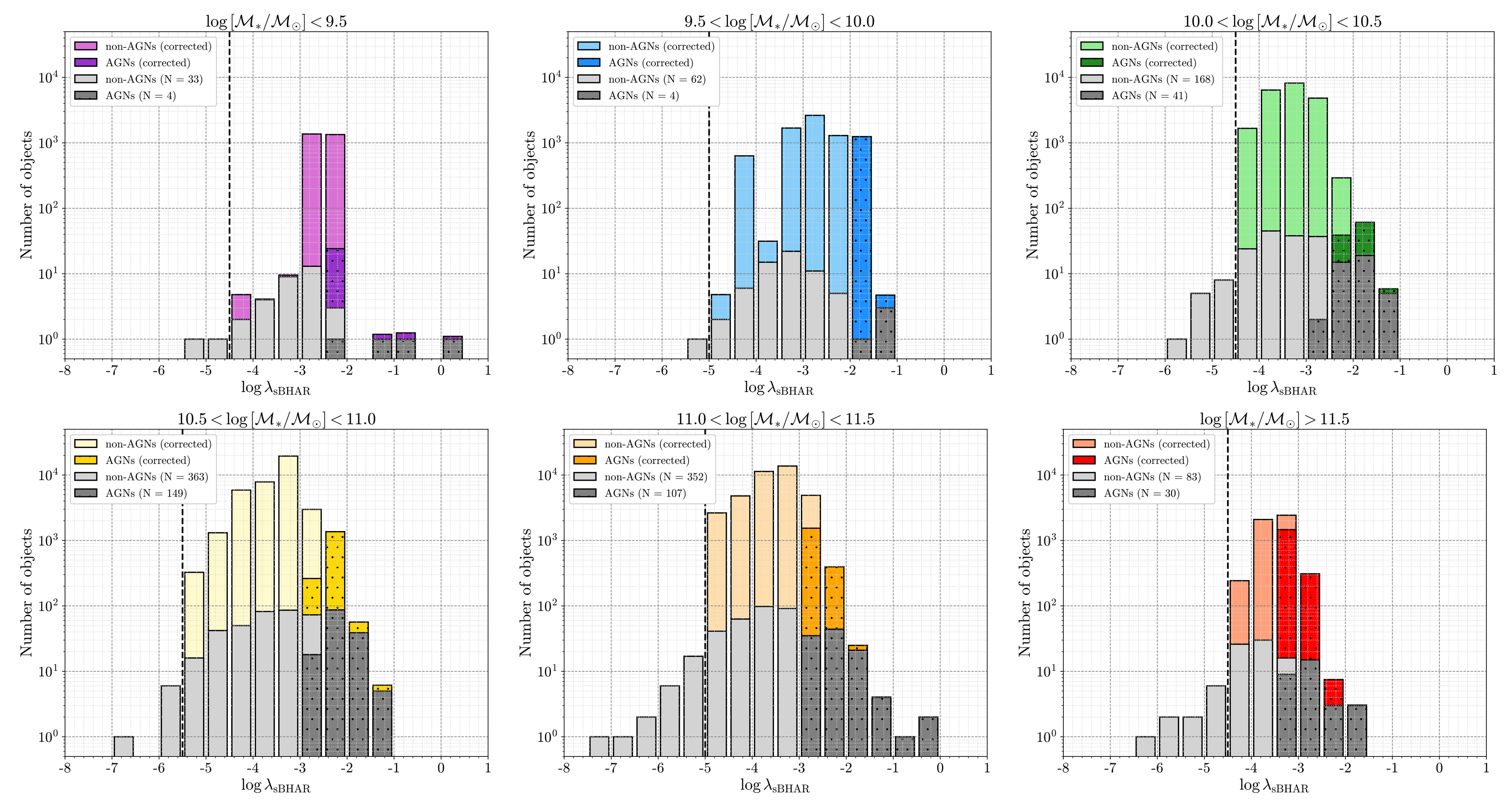

Figure 6: The distribution of the specific black hole accretion rate (sBHAR) for non-AGNs and AGNs (AGN selection criteria from Figures 2 and 3) in six $\log[\mathcal{M}_*/\mathcal{M}_\odot]$ ranges. The number of objects with certain values of sBHAR are corrected for sensitivity of detectors with flux upper-limit curves (see Fig. 5, grey color shows the uncorrected data). The black dashed line represents the limit for reliable flux upper-limit correction.

The SFR–BHAR diagrams

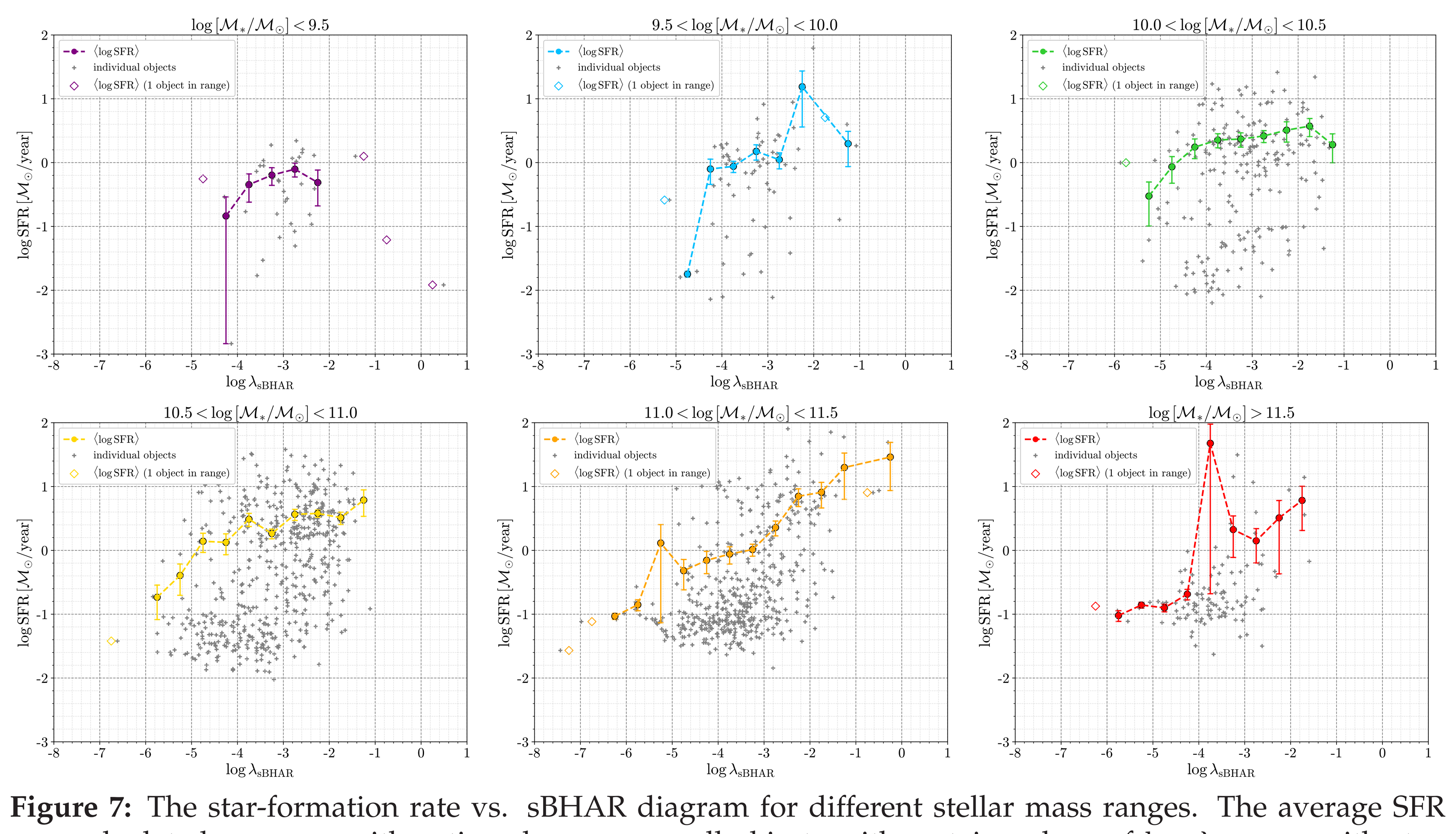

Figure 7: The star-formation rate vs. sBHAR diagram for different stellar mass ranges. The average SFR was calculated as mean arithmetic values among all objects with certain values of $\log\lambda_{\rm sBHAR}$ with step $\Delta(\log\lambda_{\rm sBHAR}) = 0.5$. The open diamonds show the value of $\langle\log{\rm SFR}\rangle$ was averaged by less than 2 objects in certain $\log\lambda_{\rm sBHAR}$ bin. The grey crosses present the position of the individual objects from our X-ray sample.

Conclusions

- The majority of AGN selected by L_X limit and X-ray/optical flux ratio criteria are distributed on SFR–$\mathcal{M}_*$ diagram at the star-formation sequence with stellar masses $\log[\mathcal{M}_*/\mathcal{M}_\odot] > 10.0$.
- We calculated the specific black hole accretion rate $\log\lambda_{\rm sBHAR}$ for objects in local Universe and found a significant population of objects that have a low $\log\lambda_{\rm sBHAR} < -2.0$, while "typical" AGNs have $\log\lambda_{\rm sBHAR} > -2.0$. The shape of $\log\lambda_{\rm sBHAR}$ distribution is close to Gaussian, the same as was shown in [2].
- The SFR–sBHAR diagrams show an increase of SFR with increase of $\log\lambda_{\rm sBHAR}$ in all stellar masses ranges.

References

[1] Aird et al. 2017, MNRAS, 465, 3390.
[2] Aird et al. 2018, MNRAS, 474, 1225.
[3] Brinchmann et al. 2004, MNRAS, 351, 1151.
[4] Ferrarese et al. 2000, ApJ, 536, 9.
[5] Gebhardt et al. 2000, ApJ, 539, 13.
[6] Lehmer et al. 2016, ApJ, 825, 7.
[7] Mineo et al. 2014, MNRAS, 437, 1698.
[8] Rosen et al. 2016, A&A, 590, A1.